Petroleum and Coal

Article **Open Access**

Study of the Effect of the Drill Pipe Planetary Motion on Pressure Loss Gradient of Two-Phase Flow at HPHT Conditions

Hicham Ferroudji[1], Nadia Messaoud[1], Zakarya Belimane[1], Ahmed Hadjadj[1], and Mohammad Azizur Rahman[2]

[1] *Laboratory of Petroleum Equipment's Reliability and Materials, Hydrocarbons and Chemistry Faculty, Boumerdes University, Boumerdes, Algeria*
[2] *Department of Petroleum Engineering, Texas A&M University at Qatar, Doha, Qatar*

Received September 16, 2023; Accepted January 18, 2024

Abstract

It is well known that the type of drill pipe motion has an important effect on the cuttings transportation process and pressure loss gradient in the annular space, in particular for horizontal and deviated wells. For that, it is needed to understand more about the effect of planetary motion on the pressure loss gradient during circulation of the drilling mud in the bottom hole of explored wells. In the present paper, the influence of the drill pipe planetary motion on the pressure loss gradient of a mixture (Ostwald-de Waele fluid with solid particles) in a turbulent regime during its circulation through an annular space is evaluated for different drilling parameters including eccentricity, rate of penetration, and solid particles size. In addition, the effect of drill pipe planetary motion for various conditions of temperature and pressure is evaluated for two types of muds water-based and oil-based. The numerical analysis revealed that an angular speed of 120 rpm of planetary motion can be considered as an optimal value in terms of pressure loss gradient. In addition, it was observed that the effect of the planetary motion on the pressure loss gradient depends mainly on the fluid temperature for both types of mud.

Keywords: *Planetary motion; Drilling fluid; Pressure loss gradient; Computational fluid dynamics (CFD); Turbulent regime.*

1. Introduction

Among the duties of drilling fluid during drilling operation is to assure efficient transportation of removed solid particles and small fragments to prevent their accumulation in the bottom hole, particularly for horizontal and deviated wells. On the other side, considering new parameters in drilling operations such as planetary motion (simultaneous rotational motion around the inner cylinder and the outer cylinder) can improve the accuracy of estimation of cuttings transport capability and would minimize Non-Productive Time (NPT). Moreover, motion type of drill pipe has a significant effect on the flow of drilling mud in the annular geometry, as well as, on the cuttings transportation process [1-10].

It is well known that the rotation of drill pipe has a crucial effect on the transportation process of cuttings through applying an erosive effect on solid particles and hence, can be transported in the main flow. For that, researchers have started to investigate the effect of drill pipe motion type on the flow of drilling fluids and their capability to transport removed cuttings.

The flow of drilling fluids through a concentric annular geometry with drillstring rotation was experimentally studied by Escudier and Gouldson [11]. It was pointed out that the rotation has an important effect that cannot be ignored. After that, Escudier *et al.* [12] and Escudier *et al.* [1] extended their research to take into consideration the drillstring eccentricity (offset of the drillstring from the concentric position). The results showed that the transition of the drillstring from the concentric to the fully eccentric position decreases the pressure gradient. Using a flow loop system, Ahmed and Miska [13] conducted an experimental analysis about the influence of eccentricity and rotation of the inner cylinder on the hydrodynamics of yield power-law fluids. Ferroudji *et al.* [3] conducted a numerical investigation about the effect of the drilltring on the pressure loss gradient of a non-Newtonian fluid flowing in both laminar and turbulent regimes. They concluded that the drilltring has a secondary effect when the flow regime switches to the turbulent regime. Recently, Nadia *et al.* [14] conducted a numerical investigation for non-Newtonian fluids flowing in annulus under high-pressure and high-temperature conditions.

On the other side, the influence of the drill pipe motion on cleaning out efficiency (multiphase flow) is addressed by several researchers. Phenomena of cuttings transport in a wellbore is modeled by Sun *et al.* [6] as a multiphase flow through an annular geometry using the Eulerian approach for various rotational speeds, fluid velocity, and inclination angles. Mohammadzadeh *et al.* [15] conducted a numerical study to verify the viscosity modifier effect on the cleaning-out efficiency of a Herschel-Bulkey fluid. In the work of Amanna and Movaghar [7], both numerical and experimental methods were adopted to analyze cuttings transport in deviated wellbores where a reasonable matching is found between them. Besides, a correlation for estimation of cuttings concentration in the entire annulus was developed in their study. A numerical study was carried out by Heydari *et al.* [16] in which they focused on the effect of eccentricity and angular speed of drill pipe on the behavior of cuttings transportation. They found that the cleaning-out of cuttings is negatively affected by the eccentricity of drill pipe. Some researchers [17-18] carried out parametric studies regarding the effect of various drilling parameters on the cleaning-out efficiency of drilling fluids. Akhshik *et al.* [19] constructed a CFD–DEM coupling to take into account the dynamic collision process (cutting–cutting, cutting–drill pipe and cutting–wall collisions). Evaluation of the carrying capacity of drilling fluids at high-pressure and high-temperature (HPHT) was carried out by Akbari and Hashemabadi [20] where they pointed out that the elevation in temperature and reduction in pressure may decrease cuttings transportation.

Besides, to consider the real motion of a drill pipe (planetary motion, whirling motion, etc…) which is eventually not a rotating motion, researchers started to evaluate the influence of this motion on drilling fluids through numerical modelling. Bicalho *et al.* [21] adopted this effect and modeled it by considering the CFD approach, however, the rotation of the drill pipe around its own axis was omitted. Ferroudji *et al.* [4] and Ferroudji *et al.* [22] considered the self-rotation of drill pipe in their modeling of planetary motion (also called orbital motion), however, in their study, only one-phase flow is addressed. They concluded that the cuttings transportation process can be enhanced once planetary motion takes place. In the study of Pang *et al.* [7], a numerical analysis about the effect of the planetary motion of drillstring on fluid cuttings mixture applied to cuttings transport phenomena was carried out.

In the present analysis, the influence of the planetary motion of drillstrng on the pressure gradient of a mixture (Ostwald-de Waele fluid in the presence of solid particles) in a turbulent regime during its circulation through an annular space is evaluated for various drilling parameters such as eccentricity, rate of penetration, and solid particles size. In addition, the effect of drill pipe planetary motion for various conditions of temperature and pressure is evaluated for both water-based and oil-based muds.

2. Methodology

In the present study, we assumed that the flow to be steady, isothermal, incompressible, and fully turbulent where the non-linear equations that describe the flow are solved with the commercial software Ansys-Fluent through an iterative process.

2.1. Flow geometry

To address the phenomena of a drilling fluid circulation via a horizontal annular geometry, the flow domain used in this study (Figure 1) is composed of an inlet, outlet, and two cylinders: the inner cylinder represents the drill pipe and the outer cylinder stands for the casing. Moreover, it is important to make sure that a fully established regime is reached after a specific distance from the inlet. For that, this distance is estimated based on the correlation of Shook and Roco [23]:

$$L_h = 0.062(R_e)D_h \tag{1}$$

where D_h represents the annular geometry hydraulic diameter and R_e is the Reynolds number of the mixture.

Since the eccentricity is included in this study, the inner pipe's eccentricity can be expressed mathematically considering the following relationship:

$$E = \frac{2\delta}{D_{OP} - D_{IP}} \tag{2}$$

where δ stands for the offset distance for the center of the outer cylinder; D_{OP} and D_{IP} represent the outer and the inner cylinders, respectively. In this study, the inner cylinder diameter is considered to be $D_{IP} = 0.0635\ m$ while the outer cylinder diameter is $D_{OP} = 0.1143\ m$.

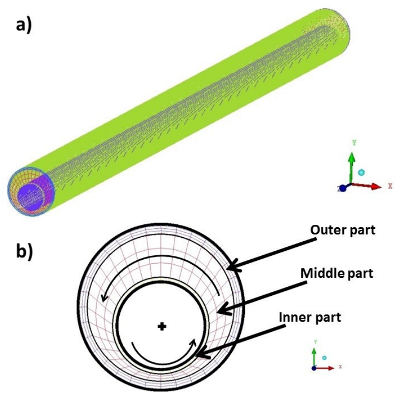

Figure 1. Generated mesh. a) 3D model. b) Mesh cross-section.

Also, the annular geometry is divided into elements using hexahedral mesh, which produces a structured mesh of the annular geometry. It is worth noting that the flow domain contains 3 parts (the part near the drillistring, the part near the casing, and the middle part) to apply the sliding mesh technique (Figure 1). This approach was used to simulate drill-string planetary motion in case of one phase flow, as described by Ferroudji *et al.* [22].

2.2. Governing equations

2.2.1. Continuity equations

The continuity equation for each phase (liquid or solid phase) can be written as (van Wachem and Almstedt [24]):

$$\frac{\partial}{\partial t}(\hbar_\alpha) + \nabla(\hbar_\alpha U_\alpha) = 0 \tag{3}$$

where (α) takes the index (l) for fluid phase and (s) in case of solids with: $\hbar_s + \hbar_l = 1$ (4)

In the case of a steady-state flow, Equation 3 becomes:

$$\nabla(\hbar_\alpha U_\alpha) = 0 \tag{5}$$

2.2.2. Momentum equations

The momentum conservation equations combining the balance of forces applied on each phase and the interphase momentum interation between the phases are written as (van Wachem and Almstedt [24]): For the fluid phase:

$$\rho_l \hbar_l \left[\frac{\partial U_l}{\partial t} + U_l \cdot \nabla U_l\right] = -\hbar_l \nabla p + \hbar_l \nabla \cdot \bar{\bar{\tau}}_l + \hbar_l \rho_l g - M \tag{6}$$

Likewise, for the solid-phase:

$$\rho_s \hbar_s \left[\frac{\partial U_s}{\partial t} + U_s \cdot \nabla U_s\right] = -\hbar_s \nabla p + \hbar_s \nabla \cdot \bar{\bar{\tau}}_l + \nabla \cdot \bar{\bar{\tau}}_s - \nabla P_s + \hbar_s \rho_s g + M \tag{7}$$

2.2.3. Closure models

a. Interphase drag force model

Assuming that cuttings are of spherical shape, the drag force per unit volume can be expressed as follows:

$$M_d = \frac{3C_D}{4d_s} \hbar_s \rho_l |U_s - U_l|(U_s - U_l) \tag{8}$$

For the case of densely distributed solid particles with a volume fraction $(\hbar_s)$ less than 0.2, the model of Wen and Yu [25] can be applied to compute the drag coefficient:

$$C_D = \mathcal{k}_l^{-1.65} \max\left[\frac{24}{N'_{Re_p}}\left(1+0.15 N'^{0.687}_{Re_p}\right), 0.44\right] \quad (9)$$

where $N'_{Re_p} = \mathcal{k}_l N_{Re_p}$ and $N_{Re_p} = \rho_l |U_l - U_s| d_s / \mu_l$

On the other hand, if ($\mathcal{k}_s$) is more than 20%, the drag model of Gidaspow [26] is used:

$$M_D = \frac{150(1-\mathcal{k}_l)^2 \mu_l}{\mathcal{k}_l d_s^2} + \frac{7}{4}\frac{(1-\mathcal{k}_l)\rho_l |U_l - U_s|}{d_s} \quad (10)$$

Based on the determined value of ($\mathcal{k}_s$), either Wen and Yu model or Gidaspow drag model is considered in the current study.

b. Lift Force Model

Since the solid particles are spherical, the Saffman and Mei lift force model (Saffman, [27]) is utilized in case of low Reynolds numbers, and the relationship is as follows:

$$M_L = \frac{3}{2\pi}\frac{\sqrt{\nu_l}}{d_s\sqrt{|\nabla \times U_l|}} C'_L \mathcal{k}_s \rho_l (U_s - U_l) \times (\nabla \times U_l + 2\Omega) \quad (11)$$

where $C'_L = 6.46$, and $0 \le N_{Re_p} \le N_{Re_\omega} \le 1$.

This correlation was expanded upon by Mei and Klausner [28] over a wider range of solid particle Reynolds numbers, as follows:

$$C'_L = \begin{cases} 6.46 \cdot f\left(N_{Re_p}, N_{Re_\omega}\right) \text{ for: } N_{Re_p} < 40 \\ 6.46 \cdot 0.0524 \cdot \left(\beta N_{Re_p}\right)^{1/2} \text{ for: } 40 < N_{Re_p} < 100 \end{cases} \text{; where:} \quad (12)$$

$$\beta = 0.5\left(N_{Re_\omega}/N_{Re_p}\right), \quad (13)$$

$$f\left(N_{Re_p}, N_{Re_\omega}\right) = (1 - 0.3314\beta^{0.5}) \cdot e^{-0.1 N_{Re_p}} + 0.3314\beta^{0.5} \text{ and} \quad (14)$$

$$N_{Re_\omega} = \rho_l \omega_l d_s^2/\mu_l, \quad \omega_l = |\nabla \times U_l| \quad (15)$$

c. Turbulence $k-\varepsilon$ Model for Multiphase Flow

Because of its robustness and reasonable accuracy for a wide range of turbulent flows (Fluent [29]), $k-\varepsilon$ turbulence model is used in this study. The finite volume method was used to numerically discretize the partial equations governing the flow. Using a suitable commercial code (ANSYS Fluent), the derived equations after discretization were repeatedly solved for each control volume while taking boundary conditions into consideration.

2.3. Fluid properties and boundary conditions

In the first part where the effect of the pressure and temperature is not considered (normal conditions), the non-Newtonian fluid is supposed to follow the power-law model. The fluid properties are shown in the Table 1. In addition, in the part where the effect of the pressure and temperature is considered, the fluid properties are obtained from the studies of William *et al.* [30] and Hermoso *et al.* [31].

Table 1. Fluid properties of the considered fluids.

		Flow consistency index "K (Pa.s^n)"	Flow behavior index "n (-)"	Yield stress "τ_0 (Pa)"
Normal conditions		0.0293	0.6	(–)
Water-based mud	10 MPa, 110°C	0.24	2.7	0.63
	10 MPa, 25°C	0.307	7.51	0.65
	0.1 MPa, 90°C	0.4	1.62	0.56
	0.1 MPa, 25°C	0.0088	1.073	0.8798
Oil-based mud	39 MPa, 140°C	0.05	0.18	0.71
	20 MPa, 100°C	0.038	0.08	0.85
	0 MPa, 40°C	0.188	0.12	0.97

For the boundary conditions, we considered the velocity inlet boundary condition at the entrance of the flow domain while a pressure outlet is specified at the outlet. Moreover, the inner cylinder is supposed to make a planetary motion through a simultaneous rotational motion around the axis of the inner cylinder as well as rotational motion around the axis of the casing. Table 2 lists the operation conditions, which are considered as input parameters for numerical simulations.

Table 2. Operation conditions.

Operation conditions	Range
Flow regime	Turbulent
ROP	[4% – 8%]
Fluid circulation velocity	[1 m/s – 2 m/s]
Inner pipe angular speed	[0 rpm – 200 rpm]
Eccentricity	[0 – 0.75]
Particles density	2550 kg/m^3
Particles diameter	[2.5 mm – 6 mm]

2.4. Sensitivity of mesh

In terms of calculation time, it is required to carry out a mesh sensitivity to determine an optimum number of mesh elements to save time, as well as, to ensure the accuracy of the obtained results. As can be seen from Figure 2, a number of 108000 elements is adopted to carry out the present analysis.

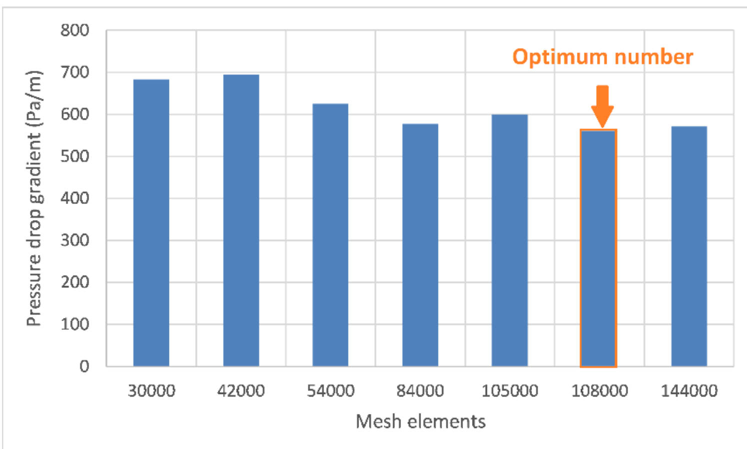

Figure 2. Evaluation of mesh sensitivity ($E = 0.5$, 100 rpm).

2.5. Simulation methodology

Ansys-Fluent Commercial code is employed to discretize the flow governing equations, and it guarantees the conservation of mass and momentum both locally for each control volume and globally over the entire flow geometry. In the current study, the Phase Coupled SIMPLE algorithm is used for all cases and it is given that the QUICK scheme is most suited for discretizing momentum equations for hexahedral elements [32]. Furthermore, the numerical simulations are carried out using a parallel computing process with 24 cores. In addition, a time step of 10^{-4} allowed to reach a convergence of 10^{-4} to 10^{-5} in all scenarios.

3. Results and discussion

3.1. Comparison with experimental data

The experimental data are obtained from the work of Ferroudji *et al.* [33] because there is a lack of experimental studies taking into account the effect of planetary motion of the inner cylinder on two-phase flow via an annular geometry. In this case, the inner part of the built mesh makes a rotational motion to be in accordance with the experimental set-up. As can be seen from Figure 3, there is a reasonable concordance between the numerical output (pressure loss gradient) and the experimental data, particularly in the range 1 m/s to 1.5 m/s. however, as the velocity increases, the discrepancy between the numerical results and experimental data increments without affecting the behavior of the pressure loss gradient.

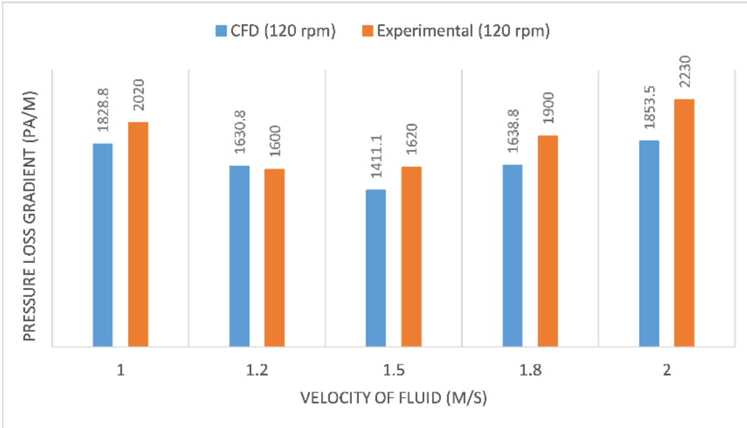

Figure 3. Comparison with experimental data.

3.2. Parametric study

The impact of the angular speed of the drill pipe on the pressure loss of the non-Newtionan fluid (power-law model) for both cases of planetary and rotational motions is depicted in Figure 4 for various flow velocities. As can be observed, in a stationary situation, there is no occurrence of a planetary motion (because planetary motion depends on angular speed and eccentricity of drill pipe) where removal of cuttings is related only to the drilling fluid flow rate. As the drilling fluid velocity increases to 1.5 m/s, the pressure loss gradient diminishes and then starts to increase because cuttings deposition is removed from the bottom side of the annular geometry. This effect is explained in the work done by Ferroudji *et al.* [33]. On the other side, with the appearance of the planetary motion, the pressure loss gradient in this situation is less than the rotational motion case, in particular for low drilling fluid velocities. For instance, at the angular speed of 120 rpm, the pressure loss gradient in the case of planetary motion is 53% and 9% less than the rotational motion for the drilling fluid velocities of 1 m/s and 1.5 m/s, respectively. This behavior can be attributed to the widening of the cross-section flow area of drilling fluid by removing deposed cutting through mechanical agitation. This effectiveness in carrying capacity is also reported in several studies [34-35].

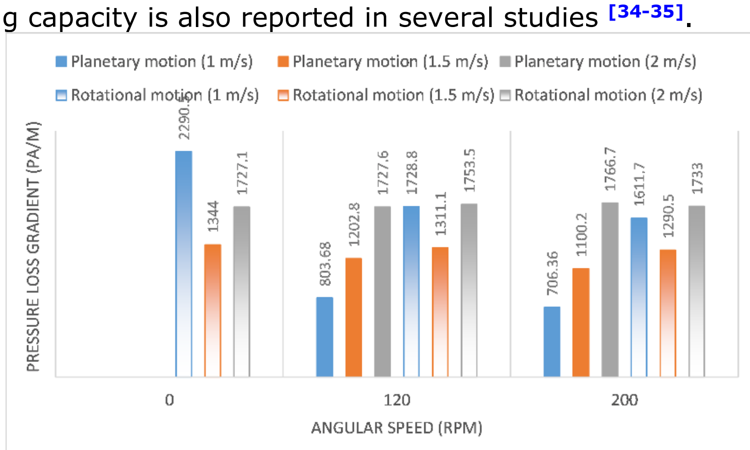

Figure 4. Effect of the angular speed of rotational and planetary motions on the pressure loss gradient for various velocities ($E = 0.5$, $ROP = 4\%$, $\kappa = 0.55$, $D_P = 2.5\,mm$, normal conditions of temperature and pressure).

Figure 5 shows the behavior of the pressure loss as a function of the drill pipe angular speed taking into account the influence of eccentricity. For the rotational motion case, an increment of the angular speed induces a decrease in the pressure loss gradient where the latter diminishes with eccentricity due to the reduction in the resistance to flow. On the other hand, a similar behavior is caused by planetary motion with smaller values of the pressure loss gradient as compared to the rotational motion situation. However, once planetary motion reaches a value of 160 rpm, the pressure loss gradient starts to increase with eccentricity. This can be attributed to the total removal of deposed cutting at high angular speeds of the drill pipe where high values of eccentricity generate important inertial effects [13] and therefore high values of pressure loss gradient.

Figure 6 indicates the variation of pressure loss when the drill pipe angular speed increases from 0 rpm to 200 rpm considering different diameters of solid particles. As shown in the Figure, for the rotational motion case, a mean reduction of 37% and 69% in pressure loss gradient are reported for the rotational motion and planetary motion cases, respectively, as the angular speed increases from 0 rpm to 200 rpm. These findings can be attributed to the increase of the cross-section area of the main flow, in particular for the planetary motion which confirms the effectiveness of the planetary motion of the drill pipe during drilling operations.

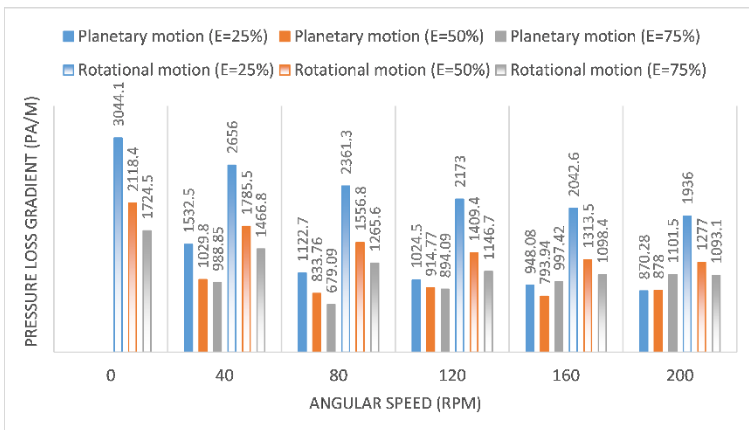

Figure 5. Effect of the angular speed of rotational and planetary motions on the pressure loss gradient for different eccentricities ($U = 1.2\, m/s$, $ROP = 4\%$, $\kappa = 0.55$, $D_P = 2.5\, mm$, normal conditions of temperature and pressure).

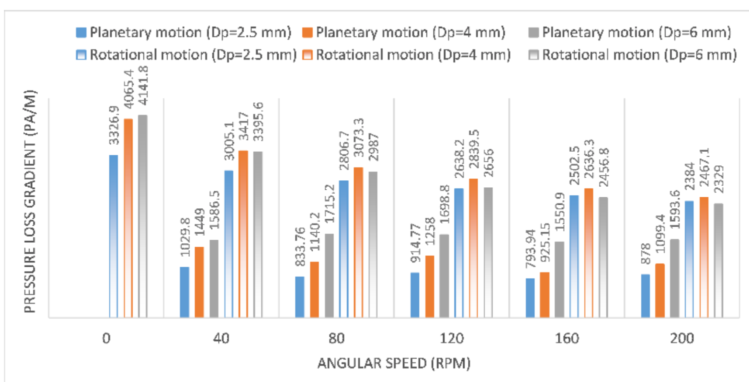

Figure 6. Effect of the angular speed of rotational and planetary motions on the pressure loss gradient for various solid particle sizes ($U = 1.2\, m/s$, $E = 0.5$, $ROP = 4\%$, $\kappa = 0.55$, normal conditions of temperature and pressure).

Figure 7 exhibits the variation of the pressure loss of the non-Newtonian fluid as a function of the drill pipe angular speed for various rates of penetration. As can be seen, an increase in the drill pipe angular speed induces a gradual decrease of the pressure loss for the rotational motion case, however, when the drill pipe makes a planetary motion, the pressure loss gradient decreases till 80 rpm, then it changes slightly for the range 80 to 200 rpm. On the other side, it can be concluded that the appearance of the planetary motion has an obvious effect on the pressure loss gradient.

Figure 8 shows the variation of pressure loss gradient of the non-Newtonian fluid as when the angular speed of the drill pipe increases for various diameter ratios. For the rotational case, it is clear that the angular speed results in a reduction of pressure loss gradient where the latter increments with the diameter ratio due to a reduction in the flow cross-section area. On the other side, when the planetary motion takes place, the pressure loss gradient is slightly influenced by the angular speed. This behavior can be explained by the absence of the secondary phase (solid particles) in this case of planetary motion. Moreover, planetary motion is not preferred for narrow annulus (high values of the diameter ratio) since it induces high pressure loss gradients.

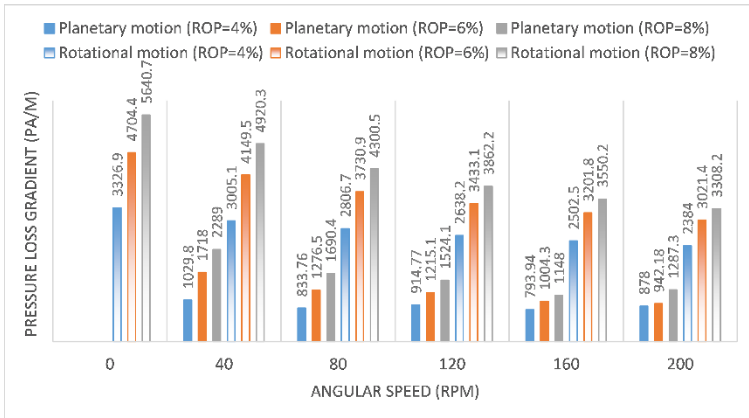

Figure 7. Effect of the angular speed of rotational and planetary motions on the pressure loss gradient for different rates of penetration ($U = 1.2\,m/s$, $E = 0.5$, $D_P = 2.5\,mm$, $\kappa = 0.55$, normal conditions of temperature and pressure).

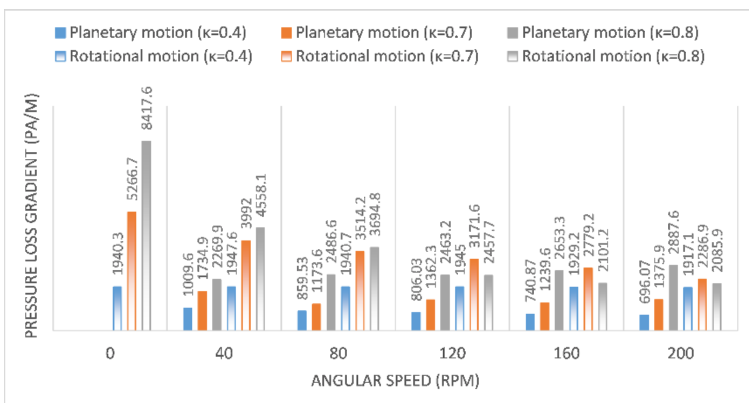

Figure 8. Effect of the angular speed of rotational and planetary motions on the pressure loss gradient for different diameter ratios ($U = 1.2\,m/s$, $E = 0.5$, $D_P = 2.5\,mm$, $ROP = 4\%$, $\kappa = 0.55$).

3.3. Impact of planetary motion for WBM and OBM

The impact of planetary motion angular speed on the pressure loss of the water-based mud for various conditions of temperature and pressure is shown in Figure 9. As can be seen from the Figure 9, at low pressure and temperature (1 bar and 25°C), the angular speed of the drillstring induces a diminishing of 33% of the pressure loss due to the enhancement of the shear-thinning effect, in particular at relatively low eccentricities ($E = 0.5$). While, for the high-pressure case (100 bar and 25°C), the pressure loss gradient increases when the angular speed of the drillstring increments because of the additional amount of pressure applied on the additional resulting in more pressure losses. In addition, the angular speed has a slight effect on the pressure loss gradient for both cases of (1 bar and 90°C) and (100 bar and

110°C) indicating that pressure in the bottom hole has a secondary influence when the temperature range is in the range of (90°C-110°C).

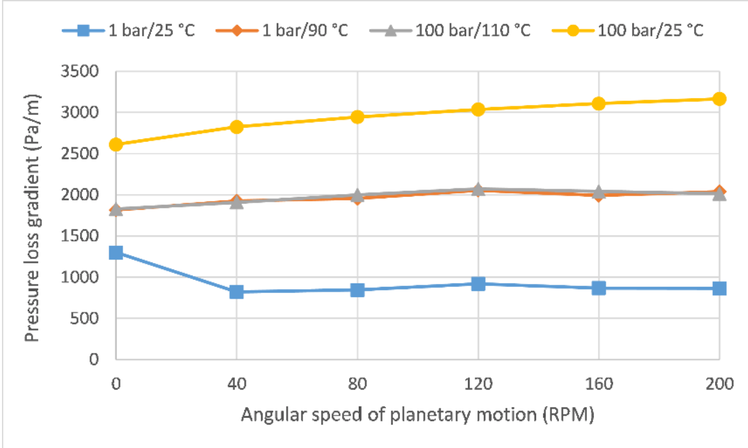

Figure 9. Effect of the angular speed of rotational and planetary motions on the pressure loss gradient of the water-based mud for various conditions of temperature and pressure ($U = 1.2\,m/s$, $E = 0.5$, $D_P = 2.5\,mm$, $ROP = 4\%$, $\kappa = 0.55$).

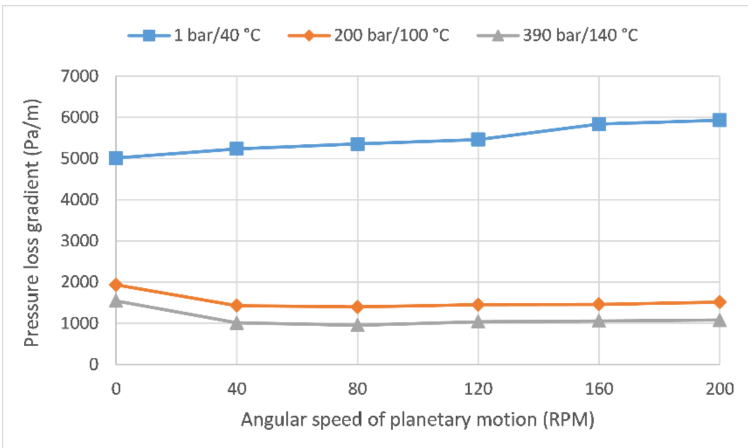

Figure 10. Effect of the angular speed of rotational and planetary motions on the pressure loss gradient of the oil-based mud for various conditions of temperature and pressure ($U = 1.2\,m/s$, $E = 0.5$, $D_P = 2.5\,mm$, $ROP = 4\%$, $\kappa = 0.55$).

Figure 10 shows the variation of the pressure loss gradient of the oil-based mud for various conditions of temperature and pressure as the angular speed of the drillstring increases. It can be seen that the planetary motion of the drillstring decreases the pressure loss gradient for high levels of temperature. Therefore, it can be concluded that the effect of the planetary motion on the pressure loss gradient depends mainly on the fluid temperature for both water-based mud and oil-based mud.

4. Conclusions

The current study uses the CFD approach to investigate the influence of the drill pipe planetary motion on the pressure loss gradient of a drilling fluid under various operation conditions including temperature and pressure. With the intensification of the planetary motion (high levels of eccentricity), an angular speed of 120 rpm of planetary motion can be considered as an optimal value in terms of the pressure loss gradient of drilling fluid. Planetary motion of drill pipe has an important role in reducing pressure loss gradient at high values of ROP. Planetary motion is not preferred for narrow annulus (high values of the diameter ratio) since it provokes high pressure loss gradients. It is found that the effect of the planetary motion on the pressure loss gradient depends mainly on the fluid temperature for both water-based mud and oil-based mud.

Acknowledgement

This publication was made possible by the grant NPRP10-0101-170091 from Qatar National Research Fund (a member of the Qatar Foundation). Statements made herein are solely the responsibility of the authors. Authors also very thankful to Minsoo Jang for helping to collect data and analysis.

Nomenclature

C_D	*Coefficient of drag (-)*
$C_{\varepsilon 1}$	*Constant for $k-\varepsilon$ model*
$C_{\varepsilon 2}$	*Constant for $k-\varepsilon$ model*
C_μ	*Constant for $k-\varepsilon$ model*
D_{OP}	*Outer cylinder diameter (m)*
D_{IP}	*Inner cylinder diameter (m)*
D_h	*Hydraulic diameter ($D_{OP}-D_{IP}$) (m)*
D_p	*Solid particles diameter (m)*
d_s	*Solid particle mean diameter (m)*
E	*Eccentricity (-)*
g	*Gravity (m/s^2)*
$\hbar_l$	*Volume fraction of liquid phase (-)*
$\hbar_s$	*Volume fraction of solid phase (-)*
K	*Consistency index ($Pa.s^n$)*
k_α	*Kinetic energy of turbulence (m^2/s^2)*
L_h	*Hydrodynamic entrance length (m)*
M	*Interphase momentum transfer*
M_d	*Drag force per unit volume (N/m^3)*
M_L	*Lift force per unit volume (N/m^3)*
n	*Behavior index (-)*
N_{Re}	*Reynolds number of fluid (-)*
N_{Re_p}	*Reynolds number of solid particles (-)*
N_{Re_ω}	*Reynolds number of vorticity (-)*
p	*Pressure of main phase (Pa)*
P_α	*Pressure of α phase (Pa)*
P_s	*Pressure of solid particles (Pa)*
Q	*Volumetric flow rate (m^3/s)*
$T_{\alpha\beta}^{(k)}$	*Interphase transfer for k*
$T_{\alpha\beta}^{(\varepsilon)}$	*Interphase transfer for ε*
U_α	*Velocity vector of α phase (m/s)*
U_l	*Velocity vector of liquid phase (m/s)*
U_s	*Velocity vector of solid phase (m/s)*
U	*Bulk velocity of liquid (m/s)*
V_c	*Total volume of solid particles (m^3)*
δ	*Inner pipe offset distance from the concentric position (m)*
ε_α	*Dissipation rate of turbulence (m^2/s^3)*
μ	*Dynamic viscosity (Pa.s)*
μ_{eff}	*Effective viscosity (Pa.s)*
$\mu_{t\alpha}$	*Phase turbulent viscosity (Pa·s)*
ρ	*Bulk density of liquid (kg/m^3)*
ρ_α	*Density of α phase (kg/m^3)*
ρ_l	*Density of liquid phase (kg/m^3)*
ρ_s	*Density of solid phase (kg/m^3)*
σ_k	*Constant for $k-\varepsilon$ turbulence model*
σ_ε	*Constant for $k-\varepsilon$ turbulence model*
$\bar{\bar{\tau}}$	*Viscous stress tensor (Pa)*
κ	*Diameter ratio (D_{IP}/D_{OP}) (-)*
Ω	*Rotation vector (1/min)*
ω	*Angular speed of inner cylinder (s^{-1})*

Abbreviation

CFD	*Computational Fluid Dynamics*
NPT	*Non-Productive time*
DEM	*Discrete Element Method*
HPHT	*High-Pressure and High-Temperature*
ROP	*Rate Of Penetration*
SIMPLE	*Semi-Implicit Method for Pressure Linked Equations*
QUICK	*Quadratic Upstream Interpolation for Convective Kinematics*
OBM	*Oil-Based Mud*
WBM	*Water-Based Mud*

Conflict of interest: *On behalf of all the co-authors, the corresponding author states that there is no conflict of interest.*

References

[1] Escudier MP, Oliveira PJ, and Pinho, FT. Fully developed laminar flow of purely viscous non-Newtonian liquids through annuli, including the effects of eccentricity and inner-cylinder rotation. Int. J. Heat Fluid Flow, 2002; 23(1): 52-73.

[2] Sorgun M. Helical flow of non-Newtonian fluids in a concentric and fully eccentric annulus. Energy Sources A: Recovery Util. Environ. Eff., 2012; 34(5): 404-412.

[3] Ferroudji H, Hadjadj A, Haddad A, and Ofei TN. Numerical study of parameters affecting pressure drop of power-law fluid in horizontal annulus for laminar and turbulent flows. J. Pet. Explor. Prod. Technol., 2019; 9(4): 3091-3101.

[4] Ferroudji H, Hadjadj A, Ofei TN, and Rahman MA. The effect of orbital motion and eccentricity of drill pipe on pressure gradient in eccentric annulus flow with Newtonian and non-Newtonian fluids. Prog. Comput. Fluid Dyn., Int. J., 2020; 20(4): 238-247.

[5] Ozbayoglu ME, Saasen A, Sorgun M, and Svanes K. Effect of pipe rotation on hole cleaning for water-based drilling fluids in horizontal and deviated wells. In IADC/SPE Asia Pacific Drilling Technology Conference and Exhibition. 2008; SPE-114965.

[6] Sun X, Wang K, Yan T, Shao S, and Jiao J. Effect of drillpipe rotation on cuttings transport using computational fluid dynamics (CFD) in complex structure wells. J. Pet. Explor. Prod. Technol., 2014; 4(3): 255-261.

[7] Amanna B, and Movaghar MRK. Cuttings transport behavior in directional drilling using computational fluid dynamics (CFD). J. Nat. Gas Sci. Eng., 2016; 34: 670-679.

[8] Pang B, Wang S, Jiang X, and Lu H. Effect of orbital motion of drill pipe on the transport of non-Newtonian fluid-cuttings mixture in horizontal drilling annulus. J. Pet. Sci. Eng., 2019; 174: 201-215.

[9] Ferroudji H, Hadjadj A, Ofei TN, Rahman MA, Hassan I, and Haddad A. CFD method for analysis of the effect of drill pipe orbital motion speed and eccentricity on the velocity profiles and pressure drop of drilling fluid in laminar regime. Petrol. Coal, 2019; 61(5): 1241-1251.

[10] Belimane Z, Hadjadj A, Ferroudji H, and Rahman MA. Modeling Surge pressures during tripping operations in a concentric annulus. Petrol. Coal, 2022; 64(2).

[11] Escudier MP, and Gouldson IW. Concentric annular flow with centerbody rotation of a Newtonian and a shear-thinning liquid. Int. J. Heat Fluid Flow, 1995; 16(3): 156-162.

[12] Escudier MP, Gouldson IW, Oliveira PJ, and Pinho FT. Effects of inner cylinder rotation on laminar flow of a Newtonian fluid through an eccentric annulus. Int. J. Heat Fluid Flow, 2000; 21(1): 92-103.

[13] Ahmed R, and Miska S. Experimental study and modeling of yield power-law fluid flow in annuli with drillpipe rotation. In SPE/IADC Drilling Conference and Exhibition. 2008; SPE-112604.

[14] Nadia M., Hadjadj A., and Ferroudji H. Numerical study of temperature and pressure effects of a yield-power law fluid flow on frictional pressure losses for laminar and turbulent regimes. Pet. Sci. Technol., 2023; 1-17.

[15] Mohammadzadeh K, Hashemabadi SH, and Akbari S. CFD simulation of viscosity modifier effect on cutting transport by oil based drilling fluid in wellbore. J. Nat. Gas. Sci. Eng., 2016; 29: 355-364.

[16] Heydari O, Sahraei E, and Skalle P. Investigating the impact of drillpipe's rotation and eccentricity on cuttings transport phenomenon in various horizontal annulus using computational fluid dynamics (CFD). J. Pet. Sci. Eng., 2017; 156: 801-813.

[17] Epelle EI, and Gerogiorgis DI. A multiparametric CFD analysis of multiphase annular flows for oil and gas drilling applications. Comput. Chem. Eng., 2017; 106: 645-661.
[18] Mohammadzadeh K, Akbari S, and Hashemabadi SH. Parametric study of cutting transport in vertical, deviated, and horizontal wellbore using CFD simulations. Pet. Sci. Technol., 2021; 39(2): 31-48.
[19] Akhshik S, Behzad M, and Rajabi M. CFD–DEM approach to investigate the effect of drill pipe rotation on cuttings transport behavior. J. Pet. Sci. Eng., 2015; 127: 229-244.
[20] Akbari S, and Hashemabadi SH. Temperature and pressure effects of drilling fluid on cutting transport using CFD simulations. Asia-Pac. J. Chem. Eng., 2017; 12(6): 980-992.
[21] Bicalho IC, Dos Santos DBL, Ataíde CH, and Duarte CR. Fluid-dynamic behavior of flow in partially obstructed concentric and eccentric annuli with orbital motion. J. Pet. Sci. Eng., 2016; 137: 202-213.
[22] Ferroudji H, Hadjadj A, Ofei TN, Gajbhiye RN, Rahman MA, Qureshi MF. Effect of drill pipe orbital motion on non-Newtonian fluid flow in an eccentric wellbore: a study with computational fluid dynamics. J. Pet. Explor. Prod. Technol., 2021; 1-20.
[23] Shook CA, and Roco MC. Slurry flow: principles and practice. Elsevier. (2013).
[24] Van Wachem BGM, Almstedt AE, Methods for multiphase computational fluid dynamics. Chem. Eng. J., 2003; 96 (1-3): 81–98.
[25] Wen CY, Yu YH. Mechanics of Fluidization. The Chemical Engineering Progress Symposium Series 1966 162, 100–111.
[26] Gidaspow D. Multiphase flow and fluidization: continuum and kinetic theory descriptions. Academic press. 1994.
[27] Saffman PGT. The lift on a small sphere in a slow shear flow. J. Fluid Mech., 1965; 22 (2): 385–400.
[28] Mei R, Klausner JF. Shear lift force on spherical bubbles. Int. J. Heat Fluid Flow, 1994; 15 (1): 62–65.
[29] Fluent ANSYS. ANSYS fluent theory guide 15.0. ANSYS, (2013). Canonsburg, PA, 33.
[30] William JKM., Ponmani S, Samuel R, Nagarajan R, and Sangwai JS. Effect of CuO and ZnO nanofluids in xanthan gum on thermal, electrical and high pressure rheology of water-based drilling fluids. J. Pet. Sci. Eng., 2014; 117: 15-27.
[31] Hermoso J, Martínez-Boza F, and Gallegos C. Combined effect of pressure and temperature on the viscous behaviour of all-oil drilling fluids. Oil & Gas Science and Technology–Revue d'IFP Energies nouvelles, 2014; 69(7): 1283-1296.
[32] Pereira FAR., Barrozo MAS, and Ataíde CH. CFD predictions of drilling fluid velocity and pressure profiles in laminar helical flow. Braz. J. Chem. Eng., 2007; 24(4): 587-595.
[33] Ferroudji H, Rahman MA, Hadjadj A, Ofei TN, Khaled MS, Rushd S, and Gajbhiye RN. 3D numerical and experimental modelling of multiphase flow through an annular geometry applied for cuttings transport. Int. J. Multiph. Flow, 2022; 151: 104044.
[34] Demiralp, Y. (2014). Effects of drill-pipe whirling motion on cuttings transport performance for horizontal drilling. Louisiana State University and Agricultural & Mechanical College.
[35] Busch A, and Johansen ST. Cuttings transport: On the effect of drill pipe rotation and lateral motion on the cuttings bed. J. Pet. Sci. Eng., 2020; 191: 107136.

To whom correspondence should be addressed: Hicham Ferroudji, Laboratory of Petroleum Equipment's Reliability and Materials, Hydrocarbons and Chemistry Faculty, Boumerdes University, Boumerdes, Algeria,
E-mail: ferroudji.h@univ-boumerdes.dz ORCID: 0000-0003-2957-4115